Carbohydrate Polymers 373 (2026) 124679

Contents lists available at ScienceDirect

Carbohydrate Polymers

journal homepage: www.elsevier.com/locate/carbpol

Towards tunable mechanical properties of *in situ* gelling chitosan hydrogels: impact of macromolecular structure including pattern of acetylation

Inès Hamouda [a,b], Maïlys Da Rocha Moreau [a,b], Lisa Basso [c], Stéphane Trombotto [c], Alexandra Montembault [c], Laurent David [c,*], Sophie Lerouge [a,b,**]

[a] Centre de Recherche du Centre Hospitalier de l'Université de Montréal (CRCHUM), Montréal, QC, Canada
[b] Departement de génie mécanique, École de technologie supérieure (ÉTS), Montréal, QC, Canada
[c] Universite Claude Bernard Lyon 1, UMR 5223, INSA Lyon, Université Jean Monnet, CNRS, Ingénierie des Matériaux Polymères, F-69622, Villeurbanne, France

ARTICLE INFO

Keywords:
Chitosan
thermosensitive hydrogel
acetylation degree
pattern of acetylation
macrostructure
Tissue engineering

ABSTRACT

Injectable *in situ* gelling physically crosslinked chitosan (CH) hydrogels allowing cell encapsulation are appealing for biomedical applications. However, the variability of the CH source is one of the major difficulties in ensuring their reproducibility. We investigated here the effect of the CH degree and pattern of acetylation (DA and PA) on its final physicochemical properties. Hydrogels made from re-acetylated CH presenting statistical repartition of repeat units along the chains, with DA of 35, 10 and 1 %, were compared to a commercial CH with DA of 10 % differing by their PA.

WAXS analysis showed different crystalline signatures depending on the PA of CH samples. Rheometry revealed faster gelation kinetics, but lower final modulus for hydrogels made of commercial *versus* statistical CH of same DA. Both also differed in terms of porosity and stability in solution. Hydrogel stiffness from 60 to 0.3 kPa were obtained by varying DA and PA. Hydrogels with the lowest DA were the most stable in solutions. Encapsulated L929 fibroblasts presented similar increasing metabolic activity over 7 days of culture within all hydrogels. This work demonstrates the relevance of controlling chitosan DA and PA for the generation of reproducible hydrogels with tunable final mechanical properties for targeted bio-applications.

Statement hypothesis: Not only the degree of acetylation (DA, *i.e.*, the molar fraction of *N*-acetyl D-glucosamine units), but also the pattern of acetylation (PA; the repartition of the acetylated/deacetylated residue sequences along the chain), can influence the mechanical properties, the porosity, and the stability of physical *in situ* gelling CH hydrogels, therefore the behavior of encapsulated cells. Indeed, when the gel is formed using weak bases (here a combination of β-glycerophosphate and sodium hydrogen carbonate), the physical crosslinking density between CH chains can be influenced by the DA and the PA due to the resulting variation of NH_2 moieties repartition.

We expect that for CH presenting a higher DA, weak gels will be generated due to reduced physical interactions established between protonated NH3+ groups and the weak base. Also, we expect to generate more stable constructs with CH presenting lower DA. Furthermore, for the same DA, the chemical process used for obtaining CH (*i.e.*, from the reacetylation of low DA CH or deacetylation of chitin under heterogeneous or homogenous conditions) yields CHs with different PA, which we presume to significantly affect final structural and mechanical properties of the obtained hydrogels. Understanding the impact of the CH macromolecular structure on its injectable *in situ* gelling hydrogel form is fundamental for the generation of suitable and reproducible CH-based hydrogel materials in biomedical applications.

* Corresponding author.
** Correspondence to: S. Lerouge, Department of mechanical engineering, École de technologie supérieure (ÉTS), 1100 Notre-Dame ouest, Montreal, H3C 1K3, QC, Canada.
E-mail addresses: laurent.david@univ-lyon1.fr (L. David), sophie.lerouge@etsmtl.ca (S. Lerouge).

https://doi.org/10.1016/j.carbpol.2025.124679
Received 19 September 2025; Received in revised form 30 October 2025; Accepted 9 November 2025
Available online 10 November 2025

1. Introduction

Chitosan (CH) hydrogels are increasingly used and envisioned for various biomedical applications, due to their high biocompatibility and tunable biodegradability (Aziz et al., 2015; Ha et al., 2018; Howard et al., 2023; Li et al., 2014; Pita-López et al., 2021; Zhou et al., 2015). Injectable *in situ* gelling physical CH hydrogels with physiological pH and rapid gelation rate are particularly appealing for minimally invasive treatments. They have been initially developed by using β-glycerophosphate (BGP) as gelling agent (Chenite et al., 2001, 2000). This weak base allows to screen CH primary amine groups and forms a CH solution at room temperature with neutral pH. When temperature increases to body temperature, a heat-induced proton transfer and hydrophobic interactions lead to gel formation (Lavertu et al., 2008). Since then, improvement in mechanical resistance and enhancement in biocompatibility have been obtained by replacing or combining BGP with sodium hydrogen carbonate (SHC) as gelling and complexation agent (Alinejad et al., 2018; Assaad et al., 2015; Komoto et al., 2019). These gels are formed by simple mixing of two solutions, leading to a solution with physiological pH and osmolarity at room temperature, to which the cells can be easily added. The solution can then be injected, and the gel forms *in situ* following the temperature increase to 37 °C. These cell-loaded hydrogels have a large potential for cell therapy and tissue engineering applications (Adoungotchodo et al., 2021; Ceccaldi et al., 2017; Monette et al., 2016).

However, due to the batch-to-batch and sourcing variability of the CH polymer, specific difficulties arise to produce CH-based hydrogel systems presenting reproducible functionalities. Even if the obtention of the CH from the deacetylation of the chitin is already a well-known process, industrialized processes may also induce variations in the purity, viscosity, weight-average molar mass (M_w) and dispersity, the mean degree of acetylation (DA) and the acetylation sequence (*i.e.*, pattern of acetylation, PA) that will impact the physicochemical properties of CH and the final properties of the CH hydrogels (*i.e.*, biodegradability, mechanical, physicochemical and biological properties) (Sorlier et al., 2001; Weißpflog et al., 2021).

Only few works already investigated the effect of the DA and M_w on CH-based hydrogels (Chenite et al., 2000; Domengé et al., 2021; Kiang et al., 2004; Molinaro et al., 2002; Sukul et al., 2021; Tavares et al., 2020; Yang et al., 2021; Zhou et al., 2008). Furthermore, investigations focusing on such *in situ* gelling CH hydrogels are scarce (Chenite et al., 2000; Molinaro et al., 2002; Zhou et al., 2008). Chenite et al. (Chenite et al., 2000) observed that the DA is a key parameter when designing injectable *in situ* gelling CH hydrogels since it affects their kinetics of gelation *in situ* in the target area and governs both the rate of degradation and the inflammatory response after implantation. Authors report a decrease of the gelling temperature with a decrease of the DA. They also showed that the hydrogels generated with CH of higher DA result in shorter residence time *in vivo*, inducing noticeable cellular inflammatory response, contrary to lower DA (*in vivo* residence up to several weeks with no detectable inflammatory response). This is also supported by Molinaro et al., (Molinaro et al., 2002), where authors also reported the decrease of the inflammatory reaction when the DA decreases, for a constant M_w. Zhou et al., (Zhou et al., 2008) described the impact of the DA and M_w on the turbidity, viscosity and *in situ* gelling properties of glycerophosphate (α and β mixtures)/CH hydrogels. They found that the microstructure of CH hydrogels, described in terms of compactness and homogeneity, was significantly impacted by the CH concentration, M_w and DA, in a complex way. While a similar effect is expected for the stronger SHC/BGP hydrogels, it was not confirmed yet.

To go a step further, the final hydrogel properties may be influenced by the repartition of the *N*-acetyl groups along the CH chain, *i.e.,* the PA. This is particularly true for physical hydrogels which properties rely on weak hydrogen or hydrophobic interactions between chains. Moreover, the acetylation sequence may also impact the ability to form crystallites, acting as physical crosslinks of high functionality. For cell therapy or tissue engineering applications, where cells are mixed with the polymer solution prior to injection and gelation, understanding the impact of the percentage and spatial distribution of *N*-acetyl groups on the gel properties is particularly important since its density and mechanical properties is likely to impact the survival and growth of the encapsulated cells.

In this context, we investigated the effect of the DA (from 1 % to 35 %), in a series of CH with a similar M_w (around 200 kg/mol) but also differing by their acetylation sequence. We thus compared re-acetylated statistical CH and a commercial deacetylated CH polymer on *i)* the gelation kinetics of the *in situ* gelling hydrogels, *ii*) the final mechanical properties, *iii*) the microstructure of the gel network, *iv*) the biodegradability within physiological media at 37 °C in presence of lysozyme and *v*) the survival and growth of encapsulated L929 fibroblasts up to 7 days. The main goal of this work was to evaluate whether or not the physicochemical and biological properties of the prepared hydrogels were DA- and PA-depend. Finally, this work aims to illustrate the importance of a precise multi-parameter macromolecular structure characterization of CHs in designing future injectable and *in situ* gelling CH hydrogels for various applications such as tissue engineering and cell therapy.

2. Material and methods

2.1. Materials

Highly deacetylated chitosan (CH) from shrimp shells (batch type 244 LG) was obtained from Mahtani Chitosan (Veraval, India). The degree of acetylation (DA) was determined by ^{1}H NMR close to 1 %. The initial weight-average molar mass (M_w) and dispersity (Đ) were 206 kg/mol and 2.3 respectively. CH (CHc10, Chitoclear, T4707, 2018) in powder form was obtained from Primex (Iceland) with DA of 10 %, M_w = 240 kg/mol and dispersity of 2.8. β-glycerol phosphate (BGP), sodium chloride, acetic acid (AcOH, > 99 $\%_{w/w}$), ammonium hydroxide (NH_4OH, 28 $\%_{w/w}$), deuterium oxide (99.9 % D) and lysozyme (CAS: 12671–19-1) were purchased from Sigma Aldrich. Sodium hydrogen carbonate (SHC) was purchased from MP Biomedicals (Solon, OH, USA). Hydrochloric acid 1 N was purchased from Thermo Fischer. Phosphate buffered saline (PBS) was purchased from Wisent INC. 1,2-propanediol and acetic anhydride were purchased from Sigma-Aldrich (Saint-Quentin-Fallavier, France). All chemicals were of reagent grade and were used without further purification.

2.2. Methods

2.2.1. Chitosan purification and reacetylation

CH was solubilized in an AcOH aqueous solution (at a polymer concentration C_p = 0.5 $\%_{w/v}$; n_{NH_2}/n_{AcOH} ~1) and successively filtered through different cellulose membranes (Millipore) with pore sizes of 3 μm, 1.2 μm and 0.45 μm. The solution was then precipitated with NH_4OH and the precipitate was washed several times by centrifugation against deionized water until neutral pH was obtained. The purified chitosan was freeze-dried and stored at room temperature (RT) until further treatment.

Purified CH of DA 1 %, from the same batch, was reacetylated in the homogeneous solution state to reach the following DA: 10 % and 35 %, using the method previously described by Vachoud et al., (Vachoud et al., 1997). Such method yields to statistical CHs (Schatz et al., 2003; Trombotto et al., 2008; Vårum et al., 1991). Briefly, low DA CH was dissolved in an AcOH aqueous solution and 1,2-propanediol was added to a ratio of 50/50 $_{(v/v)}$. Selected amounts of acetic anhydride were added for a stoichiometric reaction with D-glucosamine (GlcN) units of CH. The solution was stirred for 12 h, then the acetylated CH was precipitated, washed and freeze-dried as explained for the purification step. The DA was estimated with ^{1}H NMR (Bruker advance III, 300 MHz, 64 scans) thanks to the classical method described by (Hirai et al., 1991).

All CH samples prepared are from the same initial CH batch (either batch type 244 LG for CHs1, CHs10 and CHs35 or Chitoclear, T4707 for CHc10).

2.2.2. Size Exclusion Chromatography (SEC) analyses

Three statistical CH, with DA of 1, 10 or 35 % (CHs1, CHs10 or CHs35 respectively), prepared as described above were used in this study, and compared with a commercial deacetylated CH of DA 10 % (CHc10) presenting similar M_w (~ 200 kg/mol). The M_w and dispersity of the various CHs were determined by SEC coupled online with a differential refractometer (Optilab T-rEX, Wyatt; λ = 658 nm) and with a multiangle laser light scattering (MALLS) detector (Dawn-HELOES II, Wyatt; λ = 664 nm), as previously described (Moussa et al., 2019; Schatz et al., 2003). Briefly, CH was dissolved at a C_p = 0.5 mg/mL in AcOH/$AcONH_4$ (0.2 M/0.15 M) buffer (pH 4.5). Then, the CH solutions were eluted at a flow rate of 0.5 mL.min^{-1} (1260 infinity pump, Agilent Technologies), through two columns TSK G2500 PW and TSK G6000 PW. The value of d*n*/d*c* was determined for each polymer (0.198; 0.188; and 0.182 mL/g for DA = 1 %, 10 % and 35 % respectively), avoiding the use of standards (Schatz et al., 2003).

2.2.3. Proton nuclear magnetic resonance (^{1}H NMR) spectroscopy analyses

The pattern of acetylation (PA) of CH samples was determined by ^{1}H NMR (Brüker DRX 500 spectrometer (500 MHz) at 73 °C, 64 scans), based on a method previously described (Kumirska et al., 2009; Vårum et al., 1991). In details, 100 mg of CH were dissolved in 10 mL of HCl (0.07 M) and stirred at RT during 24 h. The solution was then treated with 5 mg of $NaNO_2$, stirred during 4 h at RT and subsequently lyophilized. Each residue of CH samples was dissolved in 1 mL of D_2O (containing 5 µL of DCl at 12 N) and then lyophilized. The procedure was repeated twice before NMR measurements to enable labile hydrogen atoms to be replaced by deuterium and to minimize the HOD signal from the solvent. Spectra were analyzed using Bruker TopSpin software (version 3.6) by fixing internal reference (δ_H 0.0 ppm) with Trimethylsilyl-3-propionic-2,2,3,3-D_4 acid sodium salt.

Data were collected from the spectra through the resonances for the protons H-1 of GlcN (D) and GlcNAc (A) units, at 4.9 and 4.6 ppm respectively. The relative experimental intensities of the diad resonances AA, DD and AD (or DA) in the CH samples were normalized according to Eqs. (1), (2) and (3):

$$F_{AD/DA} = I_{AD/DA}/(I_A + I_D) \quad (1)$$

$$F_{AA} = I_{AA}/(I_A + I_D) \quad (2)$$

$$F_{DD} = I_{DD}/(I_A + I_D) \quad (3)$$

where $I_{AD/DA}$, I_{AA}, I_{DD} are the respective experimental intensities of signals AD (or DA), AA and DD in the samples, $I_A = I_{AD/DA} + I_{AA}$ and $I_D = I_{AD/DA} + I_{DD}$. In practice, $I_{AD/DA}$ is deduced after deconvolution of the I_A peak into different components at $\delta > 4.6$ ppm (for I_{AD}) and $\delta < 4.6$ ppm (for I_{AA}). F_{AA} and F_{DD} indicate the probability that two A or D groups are adjacent to each other, whereas $F_{AD/DA}$ indicates the probability that one group A has a D neighbor, and *vice versa*. The data were transformed into one single parameter *P* according to the following Eq. (4):

$$P = F_{AD/DA}/(2F_{AA} + F_{AD/DA}) + F_{AD/DA}/(2F_{DD} + F_{AD/DA}) \quad (4)$$

The *P* values range from 0 to 2, where the interval 0–0.5 refers to a block dominated distribution, 0.5–1.5 to a random dominated distribution and 1.5–2 to an alternating dominated distribution of *N*-acetyl groups along the chitosan chain (Lopez et al., 2020). *N*-acetyl groups distribution along the CH backbone was compared between commercial and statistic CH with same DA of 10 % (Table 1).

2.2.4. Chitosan hydrogel preparation

CH was dissolved in an HCl aqueous solution to reach a polymer concentration C_p = 3.3 % $_{(w/v)}$ using a mechanical stirrer (850 rpm) during 4 h at RT. The obtained CH solution was then sterilized by autoclave (20 min at 121 °C). After cooling down, the samples were stored at 4 °C until further use. Several HCl concentrations (0.10, 0.12 and 0.14 M) were first studied to define the suitable compromise in terms of CH dissolution, hydrogel mechanical properties (Fig. S1) and cell cytotoxicity (Fig. S2). Based on these results, HCl aqueous solution at 0.12 M was then selected for this work.

In situ gelling CH hydrogels were prepared by mixing the CH solution and the gelling agents solution - a mix of BGP and SHC - followed by the addition of Dubelcco's Modified Eagle Medium (DMEM, Thermo Fisher Scientific) cell culture medium, using syringes connected by luer-lock, as already reported in previous studies (Ceccaldi et al., 2017; Touani et al., 2024). The solution obtained is injectable through small needles and catheters (Ceccaldi et al., 2017). The volume ratio of CH, gelling agents and DMEM was 0.6/0.2/0.2, forming hydrogel with a final CH concentration of 2 % $_{(w/v)}$, and concentrations of SHC and BGP of 0.075 M and 0.1 M, respectively. The gelling agent solution was previously sterilized by filtration through a 0.22 µm filter under a safety biological hood working with laminar flow. The pH of each CH solution and of the gel precursor solution immediately after mixtures at RT was measured using Denver Instrument UltraBasic pH meter and is summarized in Table 2.

After adding the gelling agents and cell culture media, the mixtures were directly used for rheological and biological tests or inserted into small molds and incubated at 37 °C overnight for complete gelation for mechanical and degradation tests.

2.2.5. Microstructural characterization of xerogels by Wide Angle X-ray diffraction (WAXS)

WAXS was performed at the ESRF (Grenoble France) on BM2-D2AM beamline (exp. Number IH-SC-1764). The air-dried hydrogel samples were studied in transmission mode, and the 2D image data were collected thanks to a WOS-S700 2D-Pixel photon counting detector (IMXPAD), located at about 23 cm of the sample. The incident photon energy was set to 15.700 keV. The data treatment consisted in spatial repositioning the active zones, masking the dead zones of the detector, normalization by the flat field, radial average over the beam center, normalization by sample transmission and subtraction of the empty cell. The scattering vector $q = \frac{4\pi.sin(\theta)}{\lambda}$ values, where 2θ is the scattering angle, were obtained after calibration with LaB_6 powder.

2.2.6. Rheological characterization of solutions and gels

The rheological behavior of solutions and gels were studied using a stress-controlled rheometer (Physica MCR301, Anton Paar, Germany) equipped with a 25 mm parallel-plate geometry (gap size of 1 mm) and

Table 1
Distribution of diad frequencies in commercial (CHc10) and reacetylated statistical (CHs10) CH determined by ^{1}H NMR spectroscopy. Results are given within 5 % of SD from ^{1}H NMR spectroscopy analysis.

Samples	DA (%)	F_{AA}	$F_{AD/DA}$	F_{DD}	*P*
CHc10	8.1 ± 1.0 %	0.038	0.095	0.867	0.605
CHs10	9.8 ± 1.0 %	0.037	0.142	0.821	0.739

Table 2
DA, M_w and Dispersity of CH samples, pH of the CH acidic solutions and of the mixtures after adding the gelling agents. Values of DA are given within 5 % of SD, M_w and Dispersity within 10 % of SD.

Sample	DA	M_w (kg.mol^{-1})	Dispersity	$pH_{CH\ solution}$	$pH_{mixture}$
CHs1	1 %	190	1.8	6.1	6.9
CHs10	10 %	190	2.3	5.7	6.8
CHc10	8 %	240	2.8	5.9	6.8
CHs35	35 %	210	2.1	2.3	6.7

connected to a circulating water bath (Julabo AWC100, Germany). The viscosities of the CH solutions and the gel mixtures were evaluated in continuous mode by applying a shear rate from 0.01 to 10 s^{-1}. Moreover, oscillatory measurements were performed to follow the evolution of the storage modulus (*G'*) of the CH hydrogels over time (time sweep) for 20 h within the linear viscoelastic regime, at a constant frequency of 1 Hz and a deformation amplitude of 1 %. The temperature was first set at 22 °C during 10 min to observe the stability at RT, followed by a rapid increase at 37 °C to mimic an injection in the body. A thin layer of low viscosity paraffin oil was added around the sample to prevent evaporation before each oscillatory measurement. After 24 h at 37 °C, a frequency sweep was then performed on the sample, at 37 °C in the frequency range from 10 to 0.01 Hz, still with a deformation amplitude of 1 %, followed by strain amplitude sweep from 1 to 1000 % at a constant frequency of 1 Hz. The strain at the limit of the linear viscoelastic region is determined from the decrease of *G'* in the strain sweep curves. The presented rheological results are examples of typical data obtained for each condition, not averages, except when indicated otherwise.

2.2.7. Mechanical properties of chitosan hydrogels from compression tests.

Compression tests were carried on a MACH-1™ Micromechanical System (Biomomentum, Laval, Canada) equipped with a 100 N load cell. Briefly, 300 µL of the CH mixture after adding the gelling agent and DMEM (*cf* section *2.2.4*) were molded in 8.6 mm diameter cylinders and incubated overnight at 37 °C prior to the measurement. The samples (about 7 mm height) were then compressed up to a nominal strain (ε) of 80 % at a deformation rate of 100 % min^{-1}. The nominal stress (σ) is calculated from the measured applied forced (*F*) and the initial sample section and then plotted *vs* ε. The elastic modulus (*E*) was obtained within the linear region by a linear regression of the stress-strain curve in the strain range from 0 and 10 %.

2.2.8. In vitro biodegradability of hydrogels

Cylinders of CH hydrogels (300 µL) were prepared as described in section *2.2.4* and *2.2.5*. After gelation overnight at 37 °C, the samples were weighted (W_0) and introduced into porous inserts (12 well plates, 8 µm, Invitrogen). The biodegradability was measured by means of mass variation following immersion at 37 °C in 2 mL of different media, namely PBS, lysozyme solution (1 mg/mL in PBS) and DMEM supplemented with 10 % of fetal bovine serum (FBS, Gibco, Thermo Fisher Scientific, Leicestershire, UK) and 1 % of penicillin/streptomycin (Wisent). Samples were weighted (W_t) every day for the next 7 days, the media being replaced by a fresh one at each time point. The relative mass variation was calculated following Eq. 5:

$$\text{Mass variation } (\%) = \frac{Wt - W0}{W0} \times 100 \quad (5)$$

2.2.9. "Porosity" observation by fluorescence microscopy

The porosity of the hydrogel networks was imaged at the micron scale and above using labelled fluorescein isocyanate chitosan (CH-FITC) through confocal microscopy. CH-FITC was prepared as described previously (Onishi & Machida, 1999). Then a low amount of CH-FITC (0.01 $\%_{w/v}$ final concentration) was introduced to the CH solution prior to gel mixing and gelation in the cylindrical molds. After 24 h of incubation in the dark at 37 °C, the network was imaged using a confocal microscope (Spinning disk, Zeiss) with 20× lens.

2.2.10. Cytocompatibility of hydrogels

To evaluate the suitability of the hydrogels to be loaded with cells for cell therapy or tissue engineering applications, cell culture experiments were performed using L929 mouse fibroblast cells (ATCC, Manassas, VA, USA). Cells were encapsulated in the various CH hydrogels by syringe mixing as described in *section 2.2.4* at a final density of 10^6 cells/mL.

A volume of 250 µL of cell-laden mixture was poured into 24-well plates and allowed to gel 10 min at 37 °C prior to the addition of 1 mL of supplemented DMEM. Hydrogels controls without cells were also prepared in the same manner using DMEM in the 3rd syringe (instead of the cell suspension). Cell culture experiments were performed at 37 °C in a humidified incubator with 5 % of CO_2 and the cell culture media was changed at day 1 and 3. Live/dead and AlamarBlue assays were performed in triplicate using three different batches of cells, as described below.

2.2.10.1. Live/dead assay. At days 1, 3 and 7, encapsulated cells were stained using Calcein AM (2 µM) and ethidium-homodimer-3 (5.5 µM, Life technologies, USA). Samples were imaged using inverted fluorescent microscope (x50 magnification, Leica DM IRB).

2.2.10.2. AlamarBlue assay. The survival and growth of encapsulated cells were also estimated through their metabolic activity using Alamar Blue (Resazurin Cell Viability Assay Kit, Biotium, USA) after 1, 3 and 7 days. The fluorescence emission intensity was measured using a microplate fluorescence reader (λ_{ex} 560 nm, λ_{em} 590 nm, BioTek Instruments Inc., Synergy 4, USA) and the metabolic activity expressed in % in reference to the result obtained at day 1 of each group.

2.2.10.3. Lactate Dehydrogenase (LDH) assay. The cytotoxicity of cell loaded hydrogels was evaluated through the release of LDH in media using the CyQUANT™ LDH Cytotoxicity Assay Kit (Thermo Fisher Scientific, USA), following the manufacturer's instructions at day 1 and 3. Absorbance emission intensity of the supernatant was measured using a microplate fluorescence reader (λ 490 nm and λ 680 nm, VANTAstar BMG LABTECH). The hydrogels with no cells encapsulated served as blank and the positive control refers to the maximum LDH released from seeded cells ($2.5 \cdot 10^5$ cells/mL) post incubation 45 min in presence of lysis buffer. The results were expressed as a percentage of the maximum LDH release from the dead cells at day 0 (corresponding to the positive control) following the Eq. (6):

$$\text{Cytotoxicity } (\%) = \frac{\lambda_{sample} - \lambda_{blank}}{\lambda_{positive\ control}} \times 100 \quad (6)$$

2.2.11. Statistical analyses

All the characterization measurements of the samples were performed in triplicate, unless otherwise specified, where *N is* the number of each independent replicate and *n* the number of samples in each *N*. Results are showed as mean ± standard deviation. Data were analyzed using two-way Analysis of Variance (ANOVA) followed by Tukey's multiple comparisons test using Prism Graph Pad software. Significance of data is presented as *, **, *** and **** for *p* values <0.05, 0.01, 0.001 and 0.0001 respectively.

3. Results

In this work, we investigated the influence of the acetylation degree (DA) and pattern of acetylation (PA) on the properties of *in situ* gelling chitosan (CH) hydrogels for cell encapsulation. We used three well-controlled statistic CHs differing by their DA following the reacetylation of the initial deacetylated CH presenting DAs of 1 % (CHs1), 10 % (CHs10) and 35 % (CHs35), as well as a commercial CH exhibiting a DA close to 10 % (CHc10) with a probable mix of bloc and statistical structure. All had a similar M_w (around 200 kg/mol).

As expected, the different CH solutions in 0.12 M HCl present different pH values (Table 2) depending on their DA. The highest DA (CHs35) has the lowest pH value (2), while decreasing the DA below 10 % led to reach pH values close to 6. At lower DA, the amine concentration is higher and play the role of a weak base capturing a significant fraction of the protons supplied by the acid. However, after mixing with the gelling agent -here a combination of β-glycerophosphate (BGP) and sodium hydrogen carbonate (SHC)-, all solutions were close to

physiological pH (between 6.75 and 6.92). The molar ratios of hydrochloric acid to amine (n_{HCl}/n_{NH2}), BGP to amine, and SHC to amine depend on the DA of CH, and are given in table S1.

3.1. Effect of the DA on rheological properties of thermogelling chitosan hydrogels

A decrease of the viscosity with the increase of the DA is observed in Fig. 1a. Statistical and high DA (CHs35 and CHs10) acidic solutions exhibit a Newtonian behavior in the entire investigated shear rate range, while CHc10 and CHs1 show a non-Newtonian behavior from shear rate of 10 s^{-1} and above.

This behavior results from the intrinsic and electrostatic contributions of the rigidity of the chains. In the polyelectrolyte solution state, such entanglement density results from the fine interplay of the protonation of amine groups, resulting from the change of pH and the pKa values with DA and ionic force (Schatz et al., 2003; Sorlier et al., 2001). Immediately after mixing with the gelling agents (and cell culture media), the gel precursor solutions present a shear-thinning behavior (possibly related to the beginning of the neutralization and complexation with the gelling agents), with viscosity varying from 10 to 0.1 Pa. s^{-1} (from shear rate 0.1 to 100 s^{-1}) confirming that the gel precursor solutions are all injectable at RT (Fig. 1b).

The gelation kinetics was monitored immediately after mixing the CH solution with the gelling agents and cell culture media, during 10 min at 22 °C to see the stability of the mixture at RT and then at 37 °C during 20 h, thus mimicking *in vivo* behavior (Fig. 1c). Initially, at 22 °C, the storage modulus (*G*') is already higher than the loss modulus (*G*") for all the samples (table S2), evidencing that the crosslinking already started at RT immediately after the mixing process. The gelation was however strongly enhanced at 37 °C, except for CHs35 which kept a low *G*' value (Fig. S3a and b). The DA has a strong impact on the starting *G*' modulus, the equilibrium moduli and the gelation kinetics at 37 °C. After 20 h, CHs35 had a much lower final *G*' (0.35 ± 0.1 Pa) and forms very weak and non-manipulable gels, in comparison with CHs10 (60 ± 8 kPa), CHs1 (8 ± 3 kPa) and CHc10 (24 ± 4 kPa) (Fig. 1d). Overall, all samples presented frequency-independent and stable values over time of *G*' and *G*" after complete gelation evidencing stable physical interactions between CH chains and the gelling agents (Fig. S3b, S3c and table S2). Surprisingly, CHs10 hydrogels were more rigid and presented a lower strain at the limit of linear viscoelastic regime (~10 %), in comparison with CHs1 and CHc10 which were softer and more deformable (limit strain of 20 and 50 % respectively) (Fig. S3d).

Such non monotonic variation in the final moduli *vs* DA may not be related to the difference of pH of the initial CH solutions, since after mixing with gelling agents and cell culture media, the resulting pH is close to 6.8 (see Table 2). The lower mechanical properties of CHs35 can possibly result from a lesser number of physical bonds able to be formed, due to a reduced number of available amine groups for complexation. Meanwhile, comparing CHs1 to CHs10 and CHc10 gels, the presence of few *N*-acetyl groups appears favorable to the formation of strong gels. Since these acetylated residues may not form complexes with the gelling agents, they may help to keep sufficient chain flexibility to favor interchain associations with complexed non-acetylated regions (Guyot et al., 2021).

3.2. Characterization of chitosans: molecular structure and semicrystalline morphology

The series of CH studied showed differences in their molecular structure (Fig. 2). The M_w are reported in Table 2, the PA was characterized by the parameter *P* from ^{1}H NMR spectra in Fig. 2a and b,

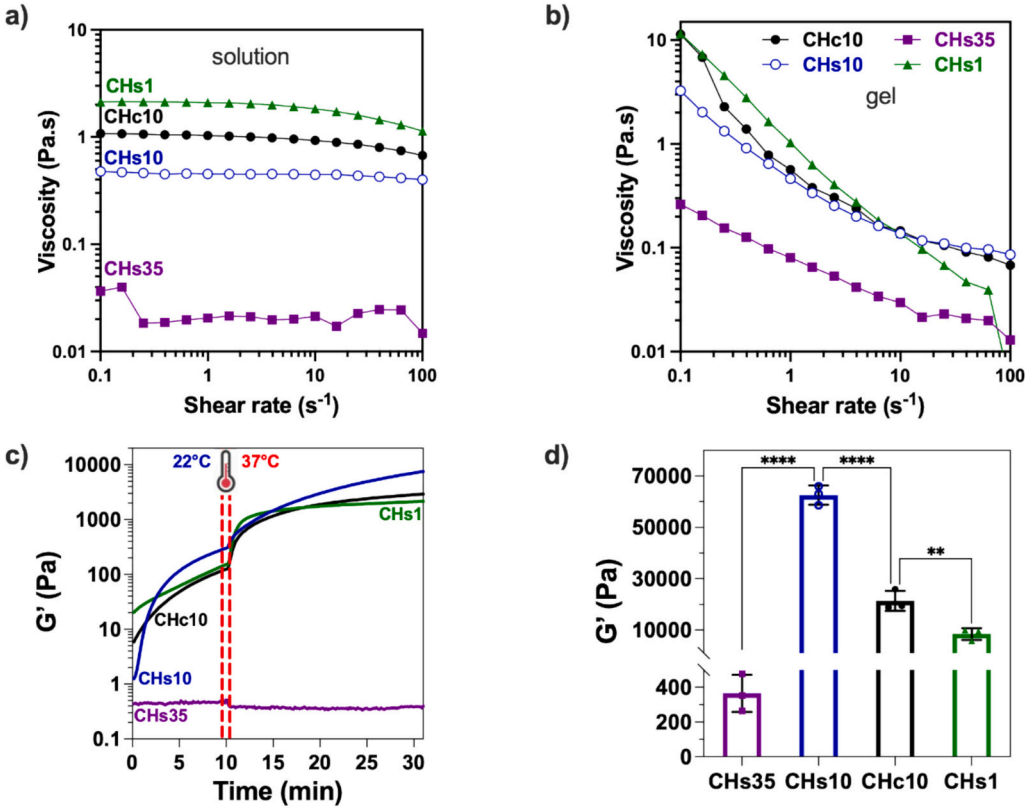

Fig. 1. Viscosity of a) CH acidic solutions at Cp = 3.3 % $_{w/v}$ in HCl 0.12 M and b) the mixtures immediately after adding the gelling agents at 22 °C showing shear thinning behavior. c) Evolution of the storage modulus (G') during the kinetics of gelation at 22 °C (during 10 min) and at 37 °C (from 10 min to 30 min) at a frequency of 1 Hz and at 1 % of deformation and d) *G*' at 20 h at 37 °C of CHs1, CHs10, CHs35 and CHc10 hydrogels (mean ± SD, *N* = 3, **, **** for $p < 0.01$ and 0.0001).

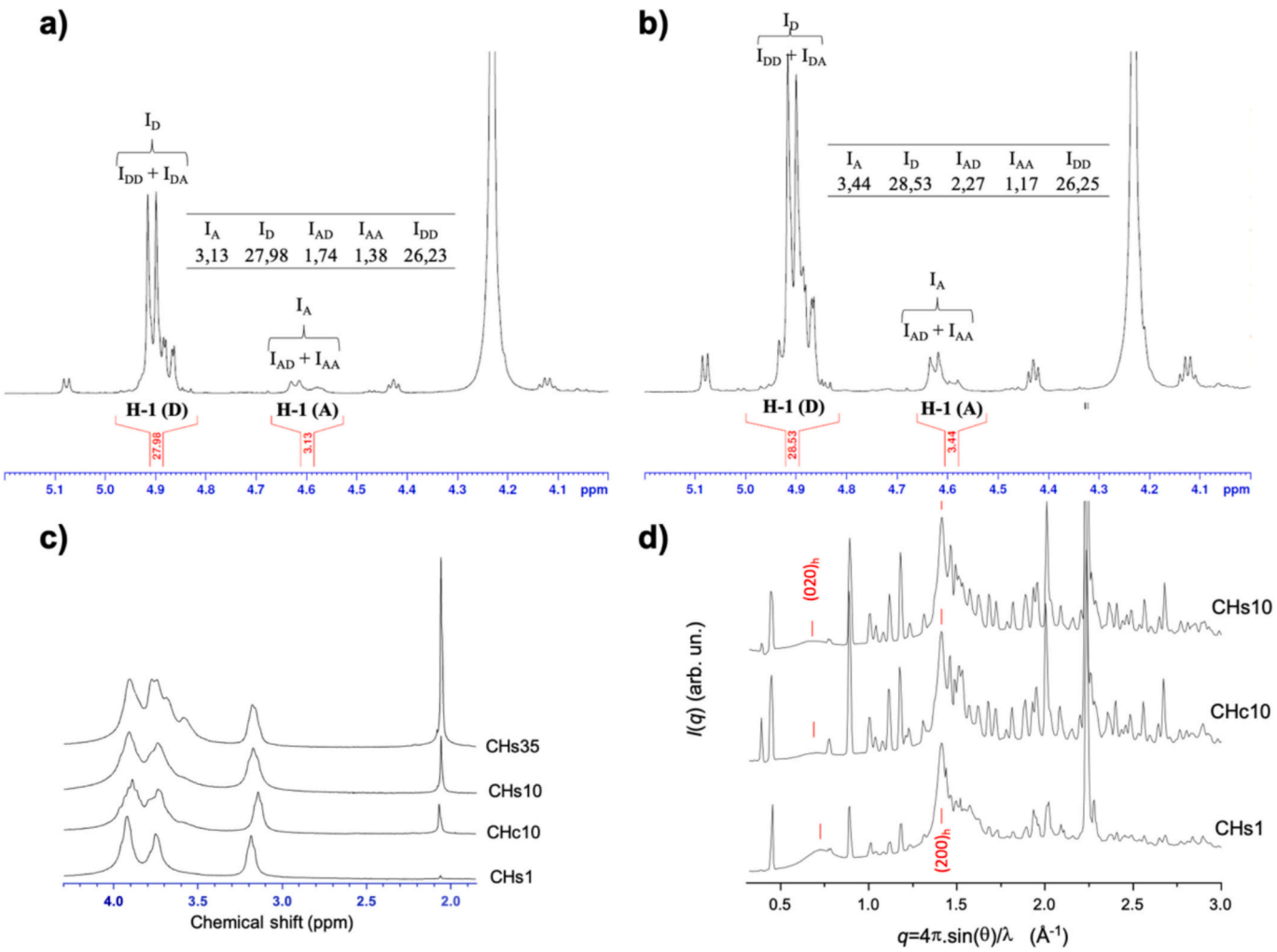

Fig. 2. ^{1}H NMR spectra of a) CHc10, b) CHs10 from 5.1 ppm to 4.1 ppm (the relative experimental intensities of the diad resonances given in the Table 1 were determined according to Eqs. (1) to (3), c) from 4.5 to 2 ppm for CHs35, CHs10, CHc10 and CHs1and d) Diffraction diagrams of xerogels obtained after air-drying of CHs1, CHs10, and CHc10 hydrogels, showing the diffraction peaks of the hydrated allomorph of CH (*i.e.* (020) and (200) reflexions) and complex salt mixture scattering. The data were normalized by the maximum intensity value of the (200) peak and shifted for clarity.

whereas the mean DA was determined by the Hirai method using the spectra from Fig. 2c. Commercial CH (CHc10), resulting from partial deacetylation of chitin exhibit a lower value of *P* (0.605) than the reacetylated CHs10 (0.739), evidencing a more statistical PA for CHs10, as expected (Table 1). The apparent 'bloc' primary structure of CHc10 compared to CHs10 could be a trace of the presence of chitin crystallites (of shrimp shells), that are less easily penetrated by the deacetylation reagents in the solid state. Since reacetylation process is performed in the solution state, with a homogeneous access to all amine groups of low DA, this leads to a more statistical distribution of D-glucosamine (GlcN) and *N*-acetyl D-glucosamine (GlcNAc) units.

The diffraction patterns of dried hydrogels (xerogels) display a strong diffraction by various salts, the indexation of which was not straightforward (Fig. 2d). The crystalline structure of CH xerogels, characterized in the dry state, is likely to be at least partly inherited from their parent hydrogels, since CH hydrogels were shown to be semi-crystalline (Pochat Bohatier et al., 2013). Here, CHs1 xerogel displayed the usual (020) and (200) peaks of the hydrated allomorph. In CHs10 and CHc10 systems, however, the (020) diffraction peaks exhibited a lower intensity and were shifted to lower *q* values, revealing a higher inter-reticular distance. Such departure from the conventional diffraction pattern of hydrated allomorph (Ogawa et al., 1984; Okuyama et al., 2000) could be due to the steric hindrance provided by complexing agents entrapped in hydrated crystals, inducing an increase of $d_{(020)}$ in the direction perpendicular to the chains. A more detailed peak shape analysis given in supplementary information (Fig. S4) reveals that CHs1 exhibits an increased $d_{020} = 8.72$ Å, whereas CHs10 and CHc10 show a clear doublet with a first refraction at the ideal structure (020) inter-reticular distance ($d_{020} = 8.488$ Å) and a shifted peak with much higher inter-reticular distances (d'_{020}–9.48 Å). This can be interpreted as a mixed crystalline structure, with complexed crystals containing acetylated residues together with BGP and/or SHC-complexed glucosamine residues. Indeed, even if -NH_2 complexation with the gelling agents is not expected to occur with *N*-acetyl D-glucosamine units, the increase of the DA from 1 to ~10 % favors the formation of the complexed crystalline structure. Furthermore, there is no *q*-shift for the (200) refection peak, showing that the insertion of the gelling agents in CH crystals is not random, and could preferentially extend between CH chains, but mostly parallel to the pyranose rings. The study of the individual impact of BGP or SHC on CH crystalline structure could possibly be studied with the preparation of formulations containing only one complexing agent but will not be addressed here.

3.3. *Microstructure of chitosan hydrogels*

Since the micro-structure of the hydrogels are important factors for cell survival and proliferation, we imaged the morphologies of the gels containing CH-FITC using confocal microscopy. While CH gels prepared

by contact with ammonia vapors or NaOH solution are known to display a capillary morphology, implying the propagation of a gel front (Sereni et al., 2017), this transitory structure was not observed here. Instead, an open, continuous microporous structure (Fig. 3) is present in all systems, suggesting some phase separation/precipitation during gelation process. The gel morphology was found to be denser for CHs10 with smaller pore size compared to its equivalent CHc10 as well as CHs1.

3.4. Stability and biodegradability of chitosan hydrogels

The stability of the hydrogels was evaluated at 37 °C in PBS, cell culture media and in PBS in presence of lysozyme (1 mg/mL) during soaking times up to 7 days (Fig. 4). All the studied hydrogels exhibited slight swelling (around 5 %) in all studied media at day 1. After 7 days in PBS (Fig. 4a), a slight mass loss (around 5 %) is observed for CHs10 and CHc10 but not for CHs1 which kept a constant mass following immersion.

In the presence of lysozyme, all hydrogels started to lose weight from day 4, the phenomenon was more pronounced for CHc10 (showing a mass loss higher than 5 %) compared to CHs1 and CHs10 (Fig. 4b). This is in agreement with the presence, in CHc10, of more sequences constituted of 3 to 4 contiguous acetylated residues that are known to play a significant role in the degradation of chitin by lysozyme. In spite of these slight differences between the hydrogel degradation kinetics, the degradation of the gels by lysozyme remains limited, possibly because the complexation/reaction of CH with gelling agents may hinder the interactions between lysozyme and CH.

Regarding the incubation in cell culture media (Fig. 4c), the swelling was almost constant, exhibiting a very slight mass loss for all the samples from day 4 to 7.

Compression tests were carried out pre- and post-immersion (Fig. 4d). Data are expressed in percentage of the Young modulus of the initial CHc10 hydrogel. After 7 days of incubation, CHs10 hydrogels were not manipulable regardless the media of immersion and therefore not measured. The rigidity of CHc10 decreased after immersion in PBS (to 40 ± 4 % of the initial value), and even more drastically in cell culture media and lysozyme media, since the hydrogel could not be manipulated anymore. Interestingly, only the CHs1 hydrogel was manipulable after immersion in all the studied media, and its rigidity (initially half compared to CHc10, about 55 ± 4 %) was not affected by immersion in cell culture media (55 ± 5 %) and only very slightly reduction in PBS (45 ± 3 %) and lysozyme media (45 ± 8 %). PBS and cell culture media may contain cations competing with the gelling agents, thus inducing a gradual decrease of the crosslink density of the samples, particularly in presence of acetylated residues statistically distributed along the chains. When the amine groups are sequenced in a more bloc distribution, as in the CHc10, or when the presence of acetyl groups is negligible, the gels are more resistant to the physicochemical alterations in high ionic force media.

3.5. Biocompatibility of chitosan hydrogels towards encapsulated cells

The survival and growth of L929 fibroblasts cells encapsulated in hydrogels were evaluated (Fig. 5). Homogenous repartition of rounded-shape cells is observed within the first day in all hydrogels (Fig. 5a). Both Live-dead images (Fig. 5a) and LDH measurements (Fig. 5b) showed low cytotoxicity within all formulations. The numbers of dead cells slightly increased from day 1 to 3, especially in CHs10. At day 3, LDH levels in CHs10 samples (9 ± 3 %) are slightly higher than CHs1 (3 ± 2 %) and CHc10 (5 ± 4 %). This could be related to its lower apparent porosity.

At day 7, cells are distributed in a cluster-like and started to elongate in CHs1, which is not observed for the other samples. However, the encapsulated cells showed similar increasing metabolic activity over days regardless of the macromolecular structure of CH (Fig. 5c). This result suggests that the encapsulated cells remained alive in all hydrogel systems, which maintained excellent biocompatibility throughout the culture period.

4. Discussion

The design of injectable *in situ* gelling cell-loaded and biodegradable scaffolds present high attractiveness in cell therapy and tissue engineering applications. The combination between CH and BGP/SHC as gelling agents allow a site-specific minimally invasive injection at neutral pH and rapid *in situ* forming implants at body temperature (Assaad et al., 2015; Ceccaldi et al., 2017). This formulation has the advantage to allow easy cell encapsulation and form quite rigid hydrogels, while avoiding any CH modification or toxic crosslinkers. Although the general impact of the DA of the CH on the mechanical properties, biodegradability and biocompatibility of lyophilizates has been already well reported (Tavares et al., 2020; Weißpflog et al., 2021), its effect on the final properties of such *in situ* gelling CH hydrogels is not yet fully reported (Chenite et al., 2000; Molinaro et al., 2002; Zhou et al., 2008).

Many variations in (*i*) the macromolecular structure parameters (*i.e.*, DA, M_w, PA) of the CH, (*ii*) the formulation parameters such as the acid used for the dissolution of the CH, the CH concentration, the viscosity of the initial CH solution, the gelling agent composition, and (*iii*) the formulation and gelation strategy, yield to different hydrogel physico- and bio-properties, which makes a thorough comparison difficult.

In this study, we were able to prepare and fully characterize well-defined and controlled statistical series of CH copolymer with DA of 1, 10 and 35 % presenting a M_w around 200 kg/mol, comparable to a commercial CH with DA of 10 %, but with a slightly different PA (*i.e.*, less statistic, with more 'block'-like pattern, Tables 1 and 2, Fig. 2). CH provided by different producers and obtained from different sources may exhibit different physico-chemical and biological behaviors, even if they exhibit the same DA, as demonstrated in this work. Reacetylation of low DA CHs, however, is a strategy to obtained series of CHs with (almost) controlled statistical patterns, thus, the variability of reacetylated batches to a given DA is largely decreased, since the deacetylation

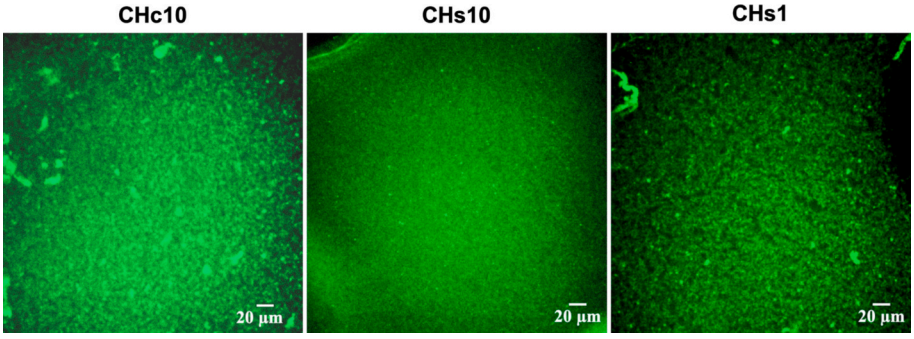

Fig. 3. Images of the network structure of the CH hydrogels obtained by confocal microscopy using FITC-CH for the preparation of hydrogels (scale bar = 20 µm) (N = 2, n = 4).

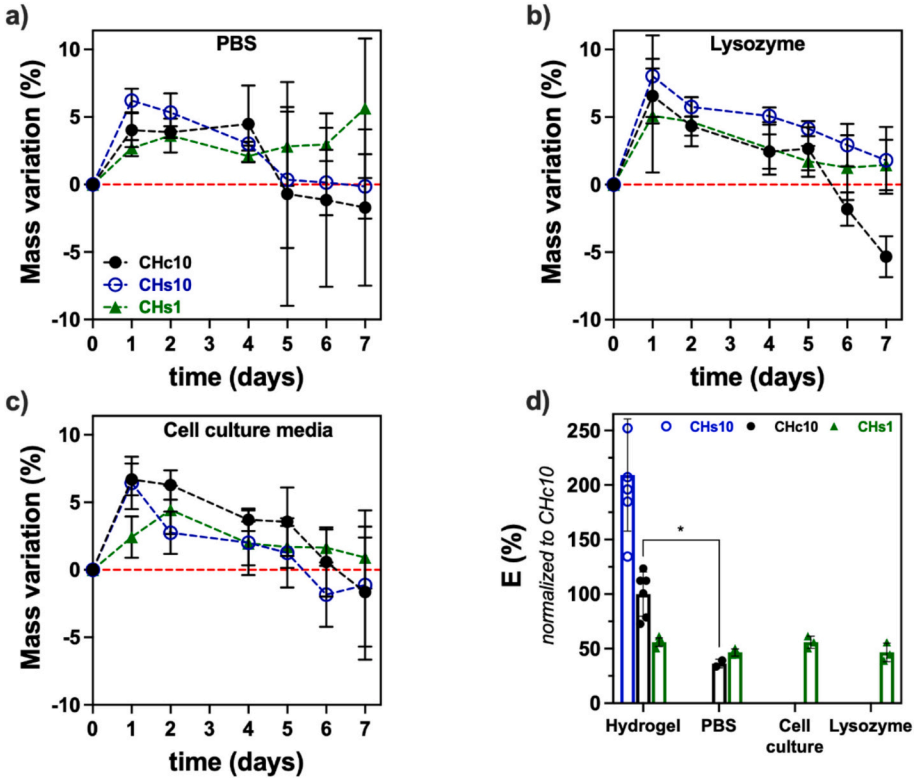

Fig. 4. Relative mass variation in % respected to initial mass of the hydrogels (around 1 g) immersed in 2 mL of a) PBS, b) in PBS with lysozyme (1 mg/mL), c) cell culture media (DMEM supplemented with 10 % FBS 1 % of penicillin/streptomycin) following incubation at 37 °C for 7 days. Dash lines are an eye indicator corresponding to the initial mass of the samples. d) Variation of the Young modulus (*E*), expressed in % of the initial CHc10 hydrogel, before and post-incubation (7 days at 37 °C) in the various solutions (PBS, lysozyme and cell culture media). Data are shown only for hydrogels that were still manipulable after incubation ($N = 3$, $n = 3$, * for $p < 0.05$).

pattern is controlled and the uncertainty of the DA is about ±3 % for the reacetylation step.

For a better comparative study, we prepared all the hydrogels by initially dissolving CH in the same acidic aqueous solvent (HCl at 0.12 M) thus ensuring sufficient protonation of all DA studied. Moreover, this HCl concentration of 0.12 M offers a good compromise between mechanical properties (Fig. S1) and biocompatibility (Fig. S2) as observed during preliminary study with CHc10. Indeed, decreasing HCl concentration to 0.10 M led to lower mechanical properties of the hydrogels. On the contrary, an increase of the HCl concentration (0.14 M) led to stiffer hydrogels but was detrimental to the biocompatibility.

To limit the factors that may influence the gelation rate (*i.e.*, CH, gelling agent concentrations and temperature), we also maintained constant the gelling agent concentration, following previously optimized formulation from our group (Alinejad et al., 2018; Assaad et al., 2015; Ceccaldi et al., 2017). After mixing the CH with the gelling agents, the crosslinking already started at 22 °C, and the kinetics increased with the temperature switch to 37 °C (Fig. 1c). Despite that, large rheological behavior differences were obtained between the CH hydrogels (Fig. 1d). Indeed, hydrogels formed with high DA (CHs35) exhibited the lowest mechanical properties ($G' = 0.35 \pm 0.1$ kPa). This was expected due to the largely smaller number of primary amine groups available for the physical crosslinks. More surprising was that gels formed with very low DA (CH1s) present lower rigidity ($G' = 8 \pm 3$ kPa) than both CH10 hydrogels (24 ± 4 and 60 ± 8 kPa for commercial and statistic respectively).

The difference between CHs10 and CHc10 emphasizes the importance of not only the DA but also the PA, characterizing the sequence of acetylated residues. CHs10 (with more randomly distributed acetylated groups) presented higher rigidity than CHc10, but was more fragile. It presented smaller pores (Fig. 3) and was also less stable in PBS compared to CHc10 (Fig. 4a). It's already well-reported that the DA influences the degradability of the CH (Pangburn et al., 1982; Sukul et al., 2021; Tomihata & Ikada, 1997). Even if all the hydrogels studied did not present any significant mass loss (Fig. 4), −except maybe for CHc10 in lysozyme after 6 days (see Fig. 4b)-, they effectively started degradation since they were not manipulable after 7 days of immersion at 37 °C (Fig. 4d).

Visually, CHs1 hydrogels were opaque in comparison to CHc10 and CHs10 which were transparent (data not shown). These observations are in accordance with a similar study involving CH hydrogels physically crosslinked with BGP where authors reported the increase of the turbidity with the DA (Zhou et al., 2008). This could be due to the occurrence of a microprecipitation process.

The higher rigidity of CHs10 *vs* CHs1 suggests that residual acetylated groups are needed to establish optimal interchain interactions for a mean DA of ~10 %. Such acetylated residues could play the role of flexible units, facilitating the association of surrounding complexed glucosamine blocks. In this sense, if the physical crosslinks in the gels (implying CH-BGP/SHC complexes) require a given acetylation sequence or acetylation sequence family involving n_D GlcN (D) and n_A GlcNAc (A) residues, it is possible to estimate such sequence composition and length, relating the probability of these bridging sequences and the probability of physical bond formation that may in turn be proportional to the (shear or Young's) elastic moduli.

In this way, assuming statistical repartition of the residues along the CH chains, several expressions can be discussed (see supplementary material) for the expression of the probability $\Pr(n_A, n_D)$ (Eq. (6)) of finding a bridging sequence constituted by n_D and n_A repeat units, such as:

$$\Pr(n_A, n_D) = C^{n_A}_{n_A+n_D} DA^{n_A} \times (1 - DA)^{n_D} \quad (6)$$

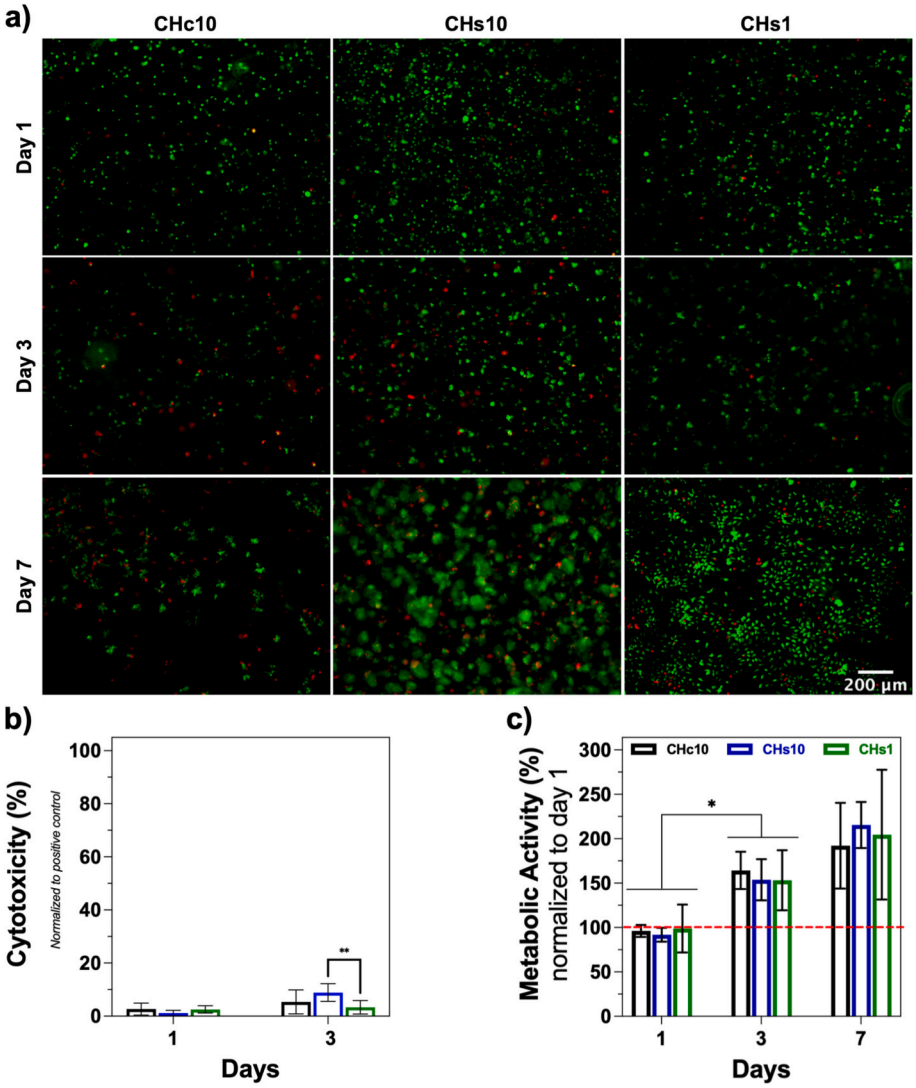

Fig. 5. a) Live/dead images, b) cytotoxicity of cell-loaded hydrogels at day 1 and 3 (LDH assays) and c) metabolic activity of encapsulated L929 fibroblast cells within CH hydrogels at day 1, 3 and 7 (AlamarBlue assays) (scale bar = 200 µm, $N = 3$ and $n = 4$; * for $p < 0.05$; ** $p < 0.01$).

And verifying the Eq. (7):

$$G'(DA) = k\,\Pr(n_A, n_D). \tag{7}$$

Thus, the DA-dependence of *G*' for statistical CH can be studied for all values of n_D and $n_A < 200$ and optimized with a least square criterion to model experimental data. This approach yields $n_D^* \sim 25$ and $n_A^* \sim 2$ (Fig. S5).

With such n_D and n_A values, the probability of appearance of such sequences in CH with DA = 1 %, 10 % and 35 % is close to be proportional to the shear moduli of the resulting gels (Fig. S5). In comparison, when shorter bridging sequences are considered (diads, triads, tetrads *etc.*.), the evolution of their fraction in statistical CH with Bernouillian statistics cannot explain the evolution of the elastic moduli of CHs1, CHs10 and CHs35. This evidences that the gelling agents-chain and interchain interaction zones in the CH gels are not restricted to one residue, but probably imply longer sequences: of about 25 residues to form the interchain interaction yielding to the hydrogels. Moreover, we have seen that in the xerogels, rather long chain portions can be complexed and form crystals with a (020) reflection shifted towards larger inter-reticular distances (Fig. 2d).

In the CHc10 system, since the acetylated units may be more often grouped together, the corresponding bridging acetylation sequences with the optimal conditions $n_D \sim 25$ and $n_A \sim 2$ may be less probable, resulting in a lower *G*', as experimentally observed (Fig. 1d). Thus, the properties of CH-BGP/SHC hydrogels seem to be highly sensitive to the DA and the PA, possibly due to the different roles of acetylated residues and glucosamine-rich chain portions contributing to the (possibly crystalline) chain junctions.

Another hypothesis for the lower rigidity of CHs1 is an insufficient number of gelling agents to screen all its positively charged amine groups (table S1), leading to some chain repulsion during physical gel formation. We have previously shown that there is an optimal SHC concentration, at which the CH hydrogels present particularly high mechanical properties (Assaad et al., 2015; Guyot et al., 2021). This is one limitation of this study: keeping the concentrations of HCl and gelling agent constant, leads to different degrees of protonation of CH chains, pH and viscosity of the CH solutions (Fig. S1) (Weißpflog et al., 2021), for which the optimal SHC concentration may vary.

Our study shows the tunability of the elastic properties of the gels by means of the DA and PA, with G' varying from 60 to 0.3 kPa, which may lead to potential application in hard, stiff and soft tissue engineering. CHs35 resulted in a weak hydrogel that may find potential in nervous tissue engineering applications. Overall, the studied formulations showed homogeneous cell repartition within the matrix and excellent

cell viability (Fig. 5). Molinaro et al., observed that a lower DA seems to favor cell biocompatibility in CH hydrogels made with BGP (Molinaro et al., 2002), in accordance with this work. Future experiments could evaluate other cell types as well as investigate further cellular phenotypes as a function of CH properties, in order to optimize CH hydrogel scaffolds for cell therapies, 3D *in vitro* models and tissue engineering applications.

5. Conclusions

The control of all key parameters of chitosan (CH) polymer preparation is essential for the design and development of medical devices based on CH-based hydrogels. We showed in this work that the control of the degree of acetylation (DA) and pattern of acetylation (PA) led to tunable mechanical properties of CH hydrogels that may fit within a wide range of tissue engineering applications. Interestingly, reacetylated and deacetylated CH of same DA present different physicochemical behaviors, due to slight differences in their PA, suggesting that the details of the molecular structure of CH play a strong role on its final physical hydrogel form. Finally, these results highlight the importance of carefully characterizing the molecular structure of CH batches prior any use in biomedical applications.

CRediT authorship contribution statement

Inès Hamouda: Writing – original draft, Methodology, Investigation, Data curation. **Maïlys Da Rocha Moreau:** Investigation, Data curation. **Lisa Basso:** Writing – review & editing, Investigation, Data curation. **Stéphane Trombotto:** Writing – review & editing, Investigation, Data curation. **Alexandra Montembault:** Writing – review & editing, Investigation, Data curation. **Laurent David:** Writing – review & editing, Supervision. **Sophie Lerouge:** Writing – review & editing, Supervision, Project administration, Funding acquisition.

Declaration of competing interest

The authors declare that they have no known competing financial interests or personal relationships that could have appeared to influence the work reported in this paper.

Acknowledgements

We thank Agnes Crepet and the Chromatography Platform of the Institut de Chimie de Lyon. We thank Francesco K. Touani for his help during cell culture experiments.

The authors thank the European Synchrotron Radiation Facility (ESRF, Grenoble) for the WAXS measurements on the BM2-D2AM beamline. The Wide-angle X-ray detector (WOS) was funded by the French National Research Agency (ANR) under the “Investissement d’Avenir” program (Grant no. ANR-11-EQPX-0010). We thank Guillaume Sudre (IMP/UCBL), Gilbert Chahine (ESRF) and Isabelle Morfin (ESRF) for their help during the WAXS experiments.

Appendix A. Supplementary data

Supplementary data to this article can be found online at https://doi.org/10.1016/j.carbpol.2025.124679.

Data availability

Data will be made available on request.

References

Adoungotchodo, A., Epure, L. M., Mwale, F., & Lerouge, S. (2021). Chitosan based hydrogel supplemented with gelatine and LINK N to enhance extracellular matrix deposition by encapsulated cells in a degenerative intervertebral disc environment. *European Cells and Materials, 40*, 471–484. https://doi.org/10.22203/eCM.v041a30

Alinejad, Y., Adoungotchodo, A., Hui, E., Zehtabi, F., & Lerouge, S. (2018). An injectable chitosan/chondroitin sulfate hydrogel with tunable mechanical properties for cell therapy/tissue engineering. *International Journal of Biological Macromolecules, 113*, 132–141. https://doi.org/10.1016/J.IJBIOMAC.2018.02.069

Assaad, E., Maire, M., & Lerouge, S. (2015). Injectable thermosensitive chitosan hydrogels with controlled gelation kinetics and enhanced mechanical resistance. *Carbohydrate Polymers, 130*, 87–96. https://doi.org/10.1016/J.CARBPOL.2015.04.063

Aziz, M. A., Cabral, J. D., Brooks, H. J. L., McConnell, M. A., Fitzpatrick, C., Hanton, L. R., & Moratti, S. C. (2015). In vitro biocompatibility and cellular interactions of a chitosan/dextran-based hydrogel for postsurgical adhesion prevention. *Journal of Biomedical Materials Research. Part B, Applied Biomaterials, 103*(2), 332–341. https://doi.org/10.1002/JBM.B.33206

Ceccaldi, C., Assaad, E., Hui, E., Buccionyte, M., Adoungotchodo, A., & Lerouge, S. (2017). Optimization of injectable thermosensitive scaffolds with enhanced mechanical properties for cell therapy. *Macromolecular Bioscience, 17*(6). https://doi.org/10.1002/mabi.201600435

Chenite, A., Buschmann, M., Wang, D., Chaput, C., & Kandani, N. (2001). Rheological characterisation of thermogelling chitosan/glycerol-phosphate solutions. *Carbohydrate Polymers, 46*(1), 39–47. https://doi.org/10.1016/S0144-8617(00)00281-2

Chenite, A., Chaput, C., Wang, D., Combes, C., Buschmann, M. D., Hoemann, C. D., … Selmani, A. (2000). Novel injectable neutral solutions of chitosan form biodegradable gels in situ. *Biomaterials, 21*(21), 2155–2161. https://doi.org/10.1016/S0142-9612(00)00116-2

Domengé, O., Ragot, H., Deloux, R., Crépet, A., Revet, G., Boitard, S. E., … Agbulut, O. (2021). Efficacy of epicardial implantation of acellular chitosan hydrogels in ischemic and nonischemic heart failure: Impact of the acetylation degree of chitosan. *Acta Biomaterialia, 119*, 125–139. https://doi.org/10.1016/J.ACTBIO.2020.10.045

Guyot, C., Cerruti, M., & Lerouge, S. (2021). Injectable, strong and bioadhesive catechol-chitosan hydrogels physically crosslinked using sodium bicarbonate. *Materials Science and Engineering: C, 118*, Article 111529. https://doi.org/10.1016/J.MSEC.2020.111529

Ha, T., Valentine, R., Moratti, S., Hanton, L., Robinson, S., & Wormald, P. J. (2018). The efficacy of a novel budesonide chitosan gel on wound healing following endoscopic sinus surgery. *International Forum of Allergy & Rhinology, 8*(3), 435–443. https://doi.org/10.1002/ALR.22057

Hirai, A., Odani, H., & Nakajima, A. (1991). Determination of degree of deacetylation of chitosan by 1H NMR spectroscopy. *Polymer Bulletin, 26*(1), 87–94. https://doi.org/10.1007/BF00299352/METRICS

Howard, J. A., Kuznietsova, H., Dziubenko, N., Aigle, A., Natuzzi, M., Thomas, E., … Tillement, O. (2023). Combating lead and cadmium exposure with an orally administered chitosan-based chelating polymer. *Scientific Reports, 13*(1). https://doi.org/10.1038/S41598-023-28968-4

Kiang, T., Wen, J., Lim, H. W., & Leong, K. W. (2004). The effect of the degree of chitosan deacetylation on the efficiency of gene transfection. *Biomaterials, 25*(22), 5293–5301. https://doi.org/10.1016/J.BIOMATERIALS.2003.12.036

Komoto, D., Furuike, T., & Tamura, H. (2019). Preparation of polyelectrolyte complex gel of sodium alginate with chitosan using basic solution of chitosan. *International Journal of Biological Macromolecules, 126*, 54–59. https://doi.org/10.1016/J.IJBIOMAC.2018.12.195

Kumirska, J., Weinhold, M. X., Sauvageau, J. C. M., Thöming, J., Kaczyński, Z., & Stepnowski, P. (2009). Determination of the pattern of acetylation of low-molecular-weight chitosan used in biomedical applications. *Journal of Pharmaceutical and Biomedical Analysis, 50*(4), 587–590. https://doi.org/10.1016/J.JPBA.2008.09.048

Lavertu, M., Filion, D., & Buschmann, M. D. (2008). Heat-induced transfer of protons from chitosan to glycerol phosphate produces chitosan precipitation and gelation. *Biomacromolecules, 9*, 640–650. https://doi.org/10.1021/bm700745d

Li, L., Wang, N., Jin, X., Deng, R., Nie, S., Sun, L., Wu, Q., Wei, Y., & Gong, C. (2014). Biodegradable and injectable in situ cross-linking chitosan-hyaluronic acid based hydrogels for postoperative adhesion prevention. *Biomaterials, 35*(12), 3903–3917. https://doi.org/10.1016/J.BIOMATERIALS.2014.01.050

Lopez, J. M., Sánchez, L. F., Nakamatsu, J., & Maruenda, H. (2020). Study of the acetylation pattern of chitosan by pure shift NMR. *Analytical Chemistry, 92*(18), 12250–12256. https://doi.org/10.1021/ACS.ANALCHEM.0C01638

Molinaro, G., Leroux, J. C., Damas, J., & Adam, A. (2002). Biocompatibility of thermosensitive chitosan-based hydrogels: An in vivo experimental approach to injectable biomaterials. *Biomaterials, 23*(13), 2717–2722. https://doi.org/10.1016/S0142-9612(02)00004-2

Monette, A., Ceccaldi, C., Assaad, E., Lerouge, S., & Lapointe, R. (2016). Chitosan thermogels for local expansion and delivery of tumor-specific T lymphocytes towards enhanced cancer immunotherapies. *Biomaterials, 75*, 237–249. https://doi.org/10.1016/J.BIOMATERIALS.2015.10.021

Moussa, A., Crépet, A., Ladavière, C., & Trombotto, S. (2019). Reducing-end “clickable” functionalizations of chitosan oligomers for the synthesis of chitosan-based diblock copolymers. *Carbohydrate Polymers, 219*, 387–394. https://doi.org/10.1016/J.CARBPOL.2019.04.078

Ogawa, K., Hirano, S., Miyanishi, T., Yui, T., & Watanabe, T. (1984). A new polymorph of chitosan. *Macromolecules, 17*(4), 973–975. https://doi.org/10.1021/MA00134A076/ASSET/MA00134A076.FP.PNG_V03

Okuyama, K., Noguchi, K., Kanenari, M., Egawa, T., Osawa, K., & Ogawa, K. (2000). Structural diversity of chitosan and its complexes. *Carbohydrate Polymers, 41*(3), 237–247. https://doi.org/10.1016/S0144-8617(99)00142-3

Onishi, H., & Machida, Y. (1999). Biodegradation and distribution of water-soluble chitosan in mice. *Biomaterials, 20*(2), 175–182. https://doi.org/10.1016/S0142-9612(98)00159-8

Pangburn, S. H., Trescony, P. V., & Heller, J. (1982). Lysozyme degradation of partially deacetylated chitin, its films and hydrogels. *Biomaterials, 3*(2), 105–108. https://doi.org/10.1016/0142-9612(82)90043-6

Pita-López, M. L., Fletes-Vargas, G., Espinosa-Andrews, H., & Rodríguez-Rodríguez, R. (2021). Physically cross-linked chitosan-based hydrogels for tissue engineering applications: A state-of-the-art review. *European Polymer Journal, 145*, Article 110176. https://doi.org/10.1016/J.EURPOLYMJ.2020.110176

Pochat Bohatier, C., Venault, A., Bouyer, D., Vachoud, L., David, L., & Faur, C. (2013). Development and characterization of composite chitosan/active carbon hydrogels for a medical application. *Journal of Applied Polymer Science, 128*(5), 2945–2953. https://doi.org/10.1002/APP.38414

Schatz, C., Viton, C., Delair, T., Pichot, C., & Domard, A. (2003). Typical physicochemical behaviors of chitosan in aqueous solution. *Biomacromolecules, 4*(3). https://doi.org/10.1021/BM025724C

Sereni, N., Enache, A., Sudre, G., Montembault, A., Rochas, C., Durand, P., … David, L. (2017). Dynamic structuration of physical chitosan hydrogels. *Langmuir: The ACS Journal of Surfaces and Colloids, 33*(44), 12697–12707. https://doi.org/10.1021/ACS.LANGMUIR.7B02997

Sorlier, P., Denuzière, A., Viton, C., & Domard, A. (2001). Relation between the degree of acetylation and the electrostatic properties of chitin and chitosan. *Biomacromolecules, 2*(3), 765–772. https://doi.org/10.1021/bm015531+

Sukul, M., Sahariah, P., Lauzon, H. L., Borges, J., Másson, M., Mano, J. F., … Reseland, J. E. (2021). In vitro biological response of human osteoblasts in 3D chitosan sponges with controlled degree of deacetylation and molecular weight. *Carbohydrate Polymers, 254*, Article 117434. https://doi.org/10.1016/J.CARBPOL.2020.117434

Tavares, L., Esparza Flores, E. E., Rodrigues, R. C., Hertz, P. F., & Noreña, C. P. Z. (2020). Effect of deacetylation degree of chitosan on rheological properties and physical chemical characteristics of genipin-crosslinked chitosan beads. *Food Hydrocolloids, 106*, Article 105876. https://doi.org/10.1016/J.FOODHYD.2020.105876

Tomihata, K., & Ikada, Y. (1997). In vitro and in vivo degradation of films of chitin and its deacetylated derivatives. *Biomaterials, 18*(7), 567–575. https://doi.org/10.1016/S0142-9612(96)00167-6

Touani, F. K., Hamouda, I., Noiseux, N., Hoesli, C., Sarkissian, S., Der, & Lerouge, S. (2024). Injectable, cryopreservable, preconditioned mesenchymal stromal cell-loaded microbeads for pro-angiogenic therapy: In vitro proof-of-concept. *Biomedical Materials*. https://doi.org/10.1088/1748-605X/AD9AF1

Trombotto, S., Ladavière, C., Delolme, F., & Domard, A. (2008). Chemical preparation and structural characterization of a homogeneous series of chitin/chitosan oligomers. *Biomacromolecules, 9*(7), 1731–1738. https://doi.org/10.1021/bm800157x

Vachoud, L., Zydowicz, N., & Domard, A. (1997). Formation and characterisation of a physical chitin gel. *Carbohydrate Research, 302*(3–4), 169–177. https://doi.org/10.1016/S0008-6215(97)00126-2

Vårum, K. M., Antohonsen, M. W., Grasdalen, H., & Smidsrød, O. (1991). Determination of the degree of N-acetylation and the distribution of N-acetyl groups in partially N-deacetylated chitins (chitosans) by high-field n.m.r. spectroscopy. *Carbohydrate Research, 211*(1), 17–23. https://doi.org/10.1016/0008-6215(91)84142-2

Weißpflog, J., Vehlow, D., Müller, M., Kohn, B., Scheler, U., Boye, S., & Schwarz, S. (2021). Characterization of chitosan with different degree of deacetylation and equal viscosity in dissolved and solid state – Insights by various complimentary methods. *International Journal of Biological Macromolecules, 171*, 242–261. https://doi.org/10.1016/J.IJBIOMAC.2021.01.010

Yang, J., Shen, M., Luo, Y., Wu, T., Wen, H., & Xie, J. (2021). Construction and characterization of Mesona chinensis polysaccharide-chitosan hydrogels, role of chitosan deacetylation degree. *Carbohydrate Polymers, 257*, Article 117608. https://doi.org/10.1016/J.CARBPOL.2020.117608

Zhou, H. Y., Chen, X. G., Kong, M., Liu, C. S., Cha, D. S., & Kennedy, J. F. (2008). Effect of molecular weight and degree of chitosan deacetylation on the preparation and characteristics of chitosan thermosensitive hydrogel as a delivery system. *Carbohydrate Polymers, 73*(2), 265–273. https://doi.org/10.1016/J.CARBPOL.2007.11.026

Zhou, H. Y., Jiang, L. J., Cao, P. P., Li, J. B., & Chen, X. G. (2015). Glycerophosphate-based chitosan thermosensitive hydrogels and their biomedical applications. *Carbohydrate Polymers, 117*, 524–536. https://doi.org/10.1016/J.CARBPOL.2014.09.094